DNA repair-pathways for DNA damages induced by particle beams

粒子線による DNA 損傷の修復メカニズム

2014

筑波大学大学院博士課程人間総合科学研究科

Human comprehensive resources of doctoral course in University of Tsukuba

Ariungerel Gerelchuluun

参考論文

Reference journal

THE PhD THESIS

DNA repair-pathways for DNA damages induced by particle beams

(粒子線による DNA 損傷の修復メカニズム)

指導教員（Supervisor）

人間総合科学研究科　医学医療系専攻　　坪井　康次　教授

Graduate School of Comprehensive Human Sciences Doctoral Program of Clinical Sciences

Koji Tsuboi　Professor

（所属）筑波大学人間総合科学研究科　疾患制御医学専攻

（Graduate School of Comprehensive Human Sciences in University of Tsukuba

Doctoral Program of Clinical Sciences）

（氏名）Ariungerel Gerelchuluun

Abstract

Purpose: To identify the roles of non-homologous end-joining (NHEJ) or homologous recombination (HR) pathways in repairing DNA double-strand breaks (DSBs) induced by high-energy protons and carbon ions (C-ions) versus γ-rays in Chinese hamster cells.

Materials and methods: The Chinese hamster ovary cell line AA8, Chinese hamster lung fibroblast cell line V79, and mutant sub-line lack in DNA-PKcs (V3), X-ray repair cross complementing protein-4 (XRCC4 (XR1)), XRCC3 (irs1SF), and XRCC2 (irs1) were exposed to γ-rays (^{137}Cs), protons (200 MeV; 2.2 keV/μm) and C-ions (290 MeV; 50 keV/μm); V3 and XR1 cells lack the NHEJ pathway whereas irs1 and irs1SF cells lack the HR pathway. After each irradiation, survival was measured using a clonogenic survival assay, *in situ* DSBs induction was evaluated via immunocytochemical analysis of histone H2A.X phosphorylation at serine 139 (γ-H2A.X foci), and chromosome aberrations were examined via solid staining.

Results: Clonogenic survival clearly depended on the NHEJ and HR pathway statuses, and the DNA-PKcs-/- cells (V3) were the most sensitive to all irradiation types. Protons and γ-rays yielded almost the same biological effects, whereas C-ion beams more enhanced the sensitivity of wild type and HR-deficient cells. However, no significant enhancement of sensitivity in cell killing was seen after C-ion irradiation for NHEJ deficient cells. Decreases in the number of γ-H2A.X foci after irradiation occurred more slowly in the NHEJ cells; in particular, V3 cells had the highest number of residual γ-H2A.X foci at 24 h after C-ion irradiation. Chromosomal aberrations were significantly higher in the NHEJ- and HR-deficient cell lines than in wild type cell lines in response to all radiation types. Protons and γ-rays induced the same aberration levels in each cell line, whereas C-ions introduced higher but not significantly different aberration levels.

Conclusions: My results suggest that the NHEJ pathway plays an important role in repairing DSBs induced by both clinical proton and C-ion beams. Furthermore, in C-ions, the HR pathway is also involved in the repair of DSBs to a greater extent as compared to γ-rays and protons.

Contents

Figures

Tables

1 Introduction

Proton and carbon ion (C-ion) beams have been applied to treat solid cancers, and the number of both treated patients and treatment facilities is increasing rapidly as a result of the excellent dose localization and preservation of surrounding normal tissues offered by this technology.

To further improve the efficacies of these particle beam radiotherapies, it is essential to clarify the molecular mechanism of both the tumor and normal tissue responses to these particle beams, since these may facilitate particle-specific radiosensitization. The biological characteristics of particle beams and photons have been analyzed and compared using different end points (*1*-*6*). Further, it has been reported that the biological effectiveness of particle beams might vary depending on the biological end points as well as the applied target tissues or cell lines (*3*, *4*) . In my previous study, I observed that proton beams induced greater rates of apoptosis than did photons, and the apoptosis induction ratios were significantly higher than the relative biological effectiveness (RBE) values calculated at 10% survival of a clonogenic survival assay (*4*). See Figure 1.1 and Table 1.1 for detail.

Gerelchuluun A et al, IJRB 2011 (*3*)

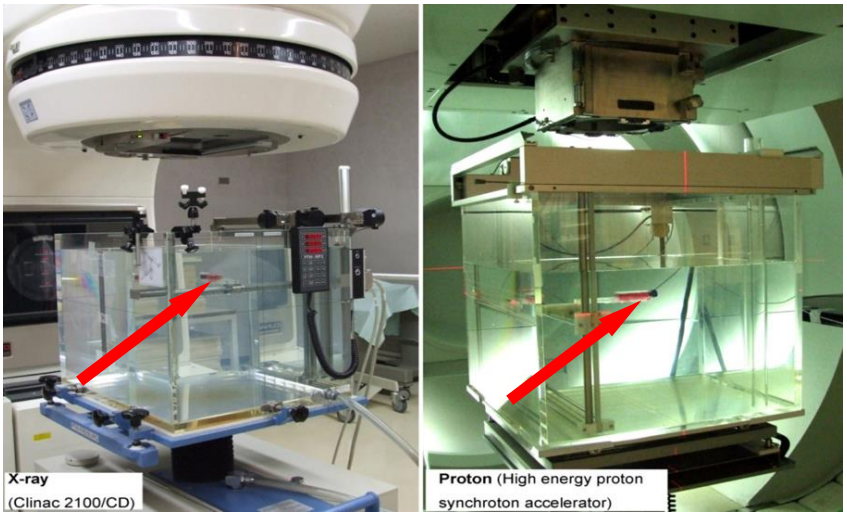

Figure 1.1. Irradiation condition for comparison of Protons and X-rays

Irradiation conditions my previous study for the 10 MV X-rays generated by Clinac 2100/CD accelerator (A) and for 200 MeV proton beams generated by PMRC synchrotron. Setup the irradiation condition very strictly, not just adjusting the dose rate, but also setting samples in the 10 cm water depth. Red arrows indicate samples in water phantom

Gerelchuluun A et al, IJRB 2011 (*4*)

Table 1.1 Comparison of Protons and X-rays

Comparison of biological effectiveness of clinically used X-rays and protons at different end points. The ratio of protons to X-rays was differ depending on end points studied and DSBs at 30 min after irradiation and apoptosis induction ratios were higher than the Relative biological effectiveness (RBE) values calculated at 10 % of clonogenic survival assay.

End points	ONS 76	MOLT4
γ-H2AX foci (30min)	1.29 (range: 1.23 – 1.37)	1.59 (range: 1.56 –1.64)
Apoptosis (12 hour)	NA	2.13 (range:1.30 – 3.22)
RBE (D_{10})	1.06 ± 0.04	1.02 ± 0.15

In addition, although C-ion beams have been shown to yield greater RBE values than protons, the characteristics of DNA lesions, and their repair mechanisms are not fully understood (*7*).

It is known that DNA double-strand breaks (DSBs) are a lethal type of damage induced by ionizing radiation, and the majority of DSBs are repaired either through the non-homologous end-joining (NHEJ) or homologous recombination (HR) pathway. Ku70/80 proteins, which are abundant in cells, instantly recognize DSB ends because of their high DNA ends affinity for these ends. In the NHEJ pathway, after Ku70/80 binds to DSB ends, DNA-PKcs is recruited to the damage sites and the XRCC4-DNA ligase IV complex subsequently re-ligates the two DSB ends (*8*). Recent reports clarified that Ku70/80 binding protects the DNA ends from unnecessary resection and inhibits HR pathway initiation (*9-11*). See Figure 1.2 for detail.

The HR pathway uses a homologous template to repair DSBs and is therefore cell cycle-dependent. HR pathway initiation is mediated by the recognition of DSB ends by the Mre11, Rad50, and Nbs1 (MRN) complex and end-resection by the CtBP-interacting protein, which associates with the MRN complex and BRCA2. Next, single-stranded DNA tails are stabilized by the RPA protein and subsequently replaced by RAD51 with the help of recombination mediators (*9, 12, 13*). See Figure 1.3 for detail.

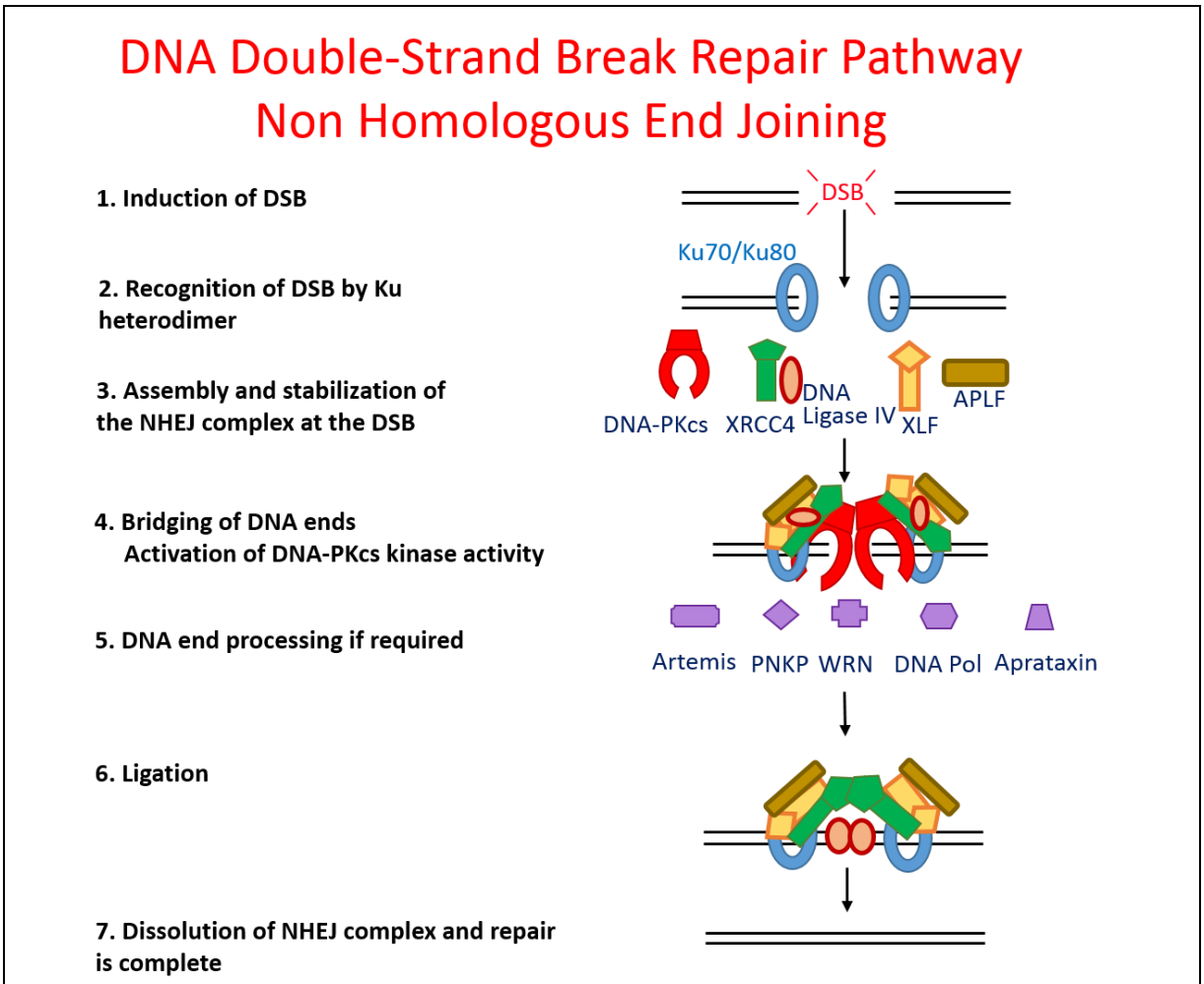

Figure 1.2. Simplified overview of Non Homologous end joining (NHEJ) pathway

NHEJ is a simple and rapid, but less accurate repair pathway. The early phase of NHEJ the Ku 70/80 proteins associates DNA ends and attratcs DNA-PKcs, which protects DNA ends against degradation and premature ligation. DNA-PKcs is known to play key role in NHEJ pathway and it activates and recruites other NHEJ proteins. The late stage of NHEJ the XRCC4-DNA ligase IV complex re-ligates the two termini of DSB.

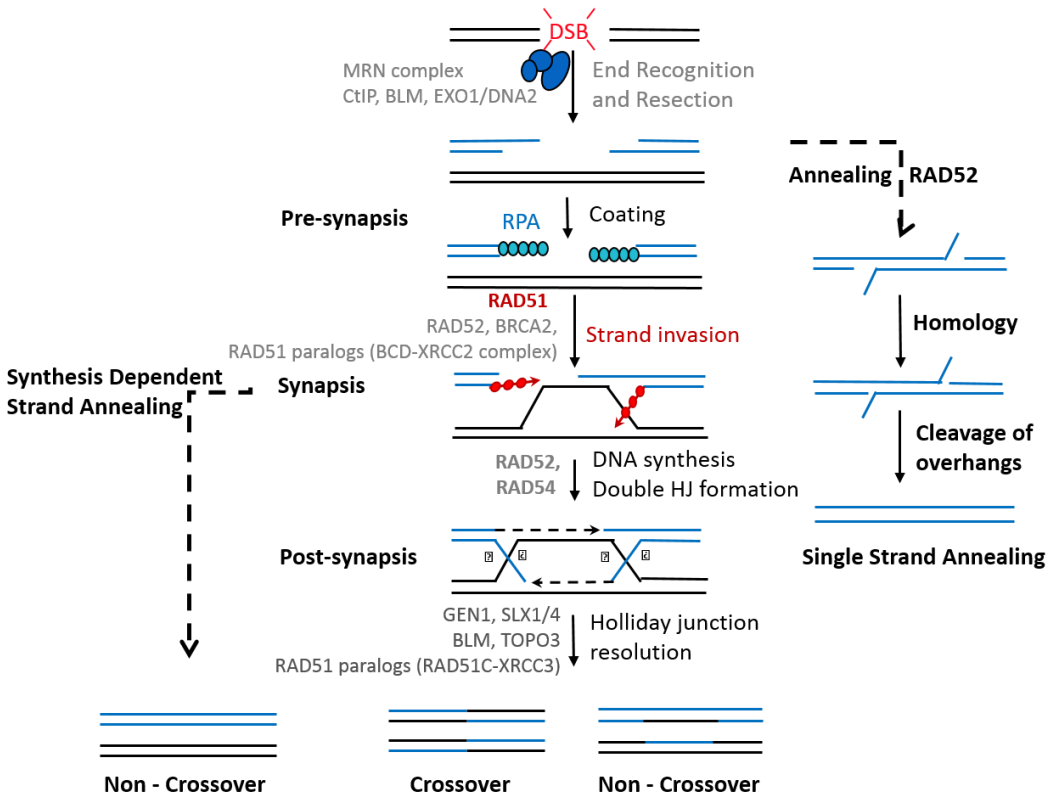

Figure 1.3. Simplified overview of Homologous Recombination (HR) pathway

HR is very accurate repair pathway, which utulizes homologous template of DNA as a guide to repair of the broken ends. The DNA ends are porcesed by MRN (Mre11/RAD50/Nbs1) complex and followed by RAD51, RAD52 and RPA associate at the processed ends to join damaged and undamaged strands. Templated guided DNA synthesis and resolution of the two strands then complete repair of the DSB.

Several reports have addressed the different contributions of the NHEJ and HR pathways to DSBs repair according to the complexity of the DSBs and the cell cycle phase in which the cells are irradiated (*14-17*). In addition, it was recently reported that high linear energy transfer (LET) particle beams induced more complex and more fragmented DNA lesions, and the involvement of HR in the repair of these lesions was greater than that observed for low LET photon irradiation lesions (*17-20*). In my preliminary experiments used high LET Iron beam irradiation, I observed that the radiosensitivity of HR deficient cells increased as the LET increases compared with NHEJ deficient cell lines (See Figure 1.4 for detail).

However, this phenomenon has not been fully confirmed because few reports have addressed the characteristics of particle beam-induced DNA lesions and the associated repair pathways. Furthermore, the contributions of the NHEJ and HR pathways to the repair of clinical proton-, C-ion-, and photon beam-induced DSBs have not been clarified.

Therefore, the purpose of this study is to identify the contributions of the NHEJ and HR pathways to the repair of proton- and C-ion-induced DNA lesions. I exposed Chinese hamster cells defective in either the NHEJ or HR pathway to γ-rays, protons, and C-ions and examined radiosensitivity, γ-H2A.X foci formation kinetics, and genome stability maintenance.

Gerelchuluun A et al, JRR, (supl-1) 2014

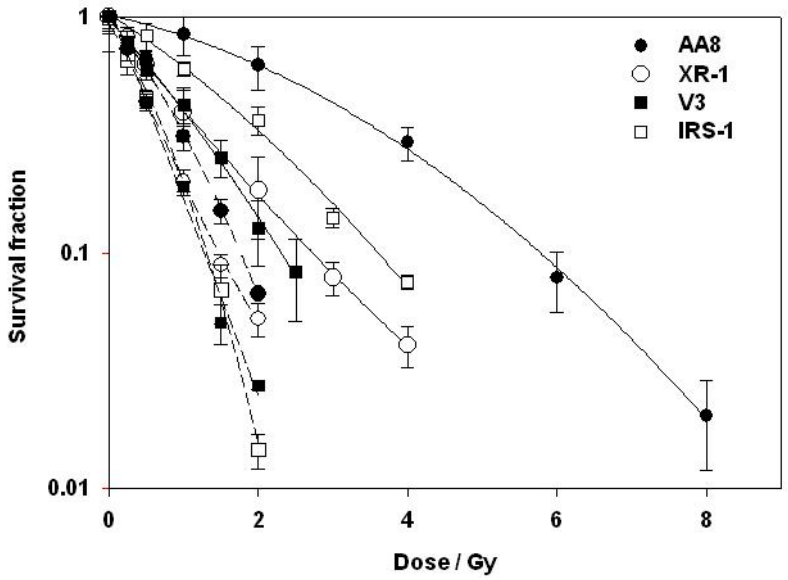

Cell line	RBE value of Iron beam
AA8	3.2
Irs1	2.7
XR1	1.8
V3	1.8

Figure 1.4. High LET Iron beams sensitizes HR deficient cell.

Clonogenic survival curves of wild type AA8 (●); NHEJ-deficient XR1 (○) and V3 (■); and HR-deficient IRS-1 (□) after irradiation with γ-rays (dashed) and Iron beams (dotted). NHEJ-deficient cells show more sensitive to γ-rays, but HR deficient cells show most sensitive to Iron beams.

2 Materials and Methods

2.1 Cell lines and culture conditions

The wild-type Chinese Hamster Ovary (CHO) cell line AA8 (*21*) and the Chinese hamster lung fibroblast cell line V79 (*22*), as well as various mutant sub-lines defective in either the NHEJ or HR pathway were used in this study. A DNA-PKcs-/- cell line (V3)(*16*) and XRCC4-/- cell line (XR1)(*23*)lacked the NHEJ pathway, whereas an XRCC3-/- cell line (irs1SF)(*24*) and XRCC2-/- cell line (irs1) (*25*) lacked the HR pathway. The irs1SF cell line was a kind gift from Dr. Takamitsu Kato at Colorado State University. See Figure 2.1 for details.

Cells were grown in minimum essential medium (Sigma-Aldrich, Tokyo, Japan) supplemented with 100µg/mL streptomycin, 100U/mL penicillin (Sigma-Aldrich), and 10% fetal bovine serum (Sigma-Aldrich). For cell transfer, the cells were rinsed with Ca^{2+} and Mg^{2+}-free phosphate buffered saline (PBS (-); Sigma-Aldrich) and dispersed in 0.25% trypsin solution containing 0.5mM ethylenediaminetetraacetate (EDTA; Sigma-Aldrich).

The cells were maintained at 37°C in a humidified incubator under 5% CO_2. The doubling times of all cell lines ranged from 16 to 20 h. The number of cells was determined using a T10 Automated Cell Counter (Bio-Rad, Tokyo, Japan). For irradiation in a sub-confluent state, the cells were seeded into either T75 or T25 flasks (NUNC; Thermo Fisher Scientific, Roskilde, Denmark) or onto glass cover slips (MATSUNAMI Glass Ind., Ltd, Osaka, Japan) in 6-well plates, and subsequently, incubated for at least 24 h for clonogenic survival assay and chromosome aberration analysis; and 48 h for γ-H2A.X foci assay under the conditions described above.

Table 2.1 The cell charactersitic and description.

NHEJ – non homologous end joining; HR – homologous repair; XRCC - X-ray repair cross complementing protein; DNA-PKcs - DNA-dependent protein kinase, catalytic subunit; PE – plating efficiency;

Cell name	Origin	Defective gene	Doubling time (hours)	PE% ± SD	Chromosome number
Wild Type					
V79	Chinese Hamster lung fibroblast	-	16.4	90.8 ± 22.8	21
AA8	Chinese Hamster ovarian	-	19.5	71.1 ± 9.5	21
HR deficient					
irs1	Chinese Hamster lung fibroblast	XRCC2	17.5	100.5 ± 12.7	19
irs1SF	Chinese Hamster ovarian	XRCC3	ND	53.7 ± 5.5	20
NHEJ deficient					
XR1	Chinese Hamster ovarian	XRCC4	18.8	46.8 ± 10.9	20
V3	Chinese Hamster ovarian	DNA-PKcs	ND	45.7 ± 11.0	21

2.2 Irradiation

2.2.1 Dosimetry

For 137Cs γ-ray irradiation, Gamma cell 40 (Atomic Energy of Canada, Ontario, Canada) was used. The dose rate was 0.76 Gy/min, which was calculated from the decay curve of the137Cs source.

For proton beam irradiation, 200-MeV proton beams were generated by the synchrotron at the Proton Medical Research Center (PMRC), University of Tsukuba, Japan. Proton dosimetry was measured as previously described (*26*, *27*). Based on the 200-MeV proton beam dose distribution, the absorbed dose was measured at the middle of the 6-cm wide spread-out Bragg peak (SOBP) using a dosimeter (0.2 cc C-110 Farmer Chamber; Applied Engineering Inc., Tokyo, Japan). The estimated energy spread and dose-average LET values at the mid-SOBP were 0–60 MeV and 2.2 keV/μm, respectively (*27*, *28*).

For C-ion beam irradiation, 290-MeV/n C-ion beams were generated by the synchrotron at the Heavy Ion Medical Accelerator in Chiba (HIMAC), National Institute of Radiological Sciences, Japan. Details concerning the beam characteristics, biological irradiation procedures, and C-ion beam dosimetry have been previously described (*29*, *30*). The experimental dose distributions were measured at the middle of a 6-cm SOBP of C-ions, the energy spread and the dose-average LET values were approximately 0-160 MeV and 50 keV/μm, respectively (*7*).

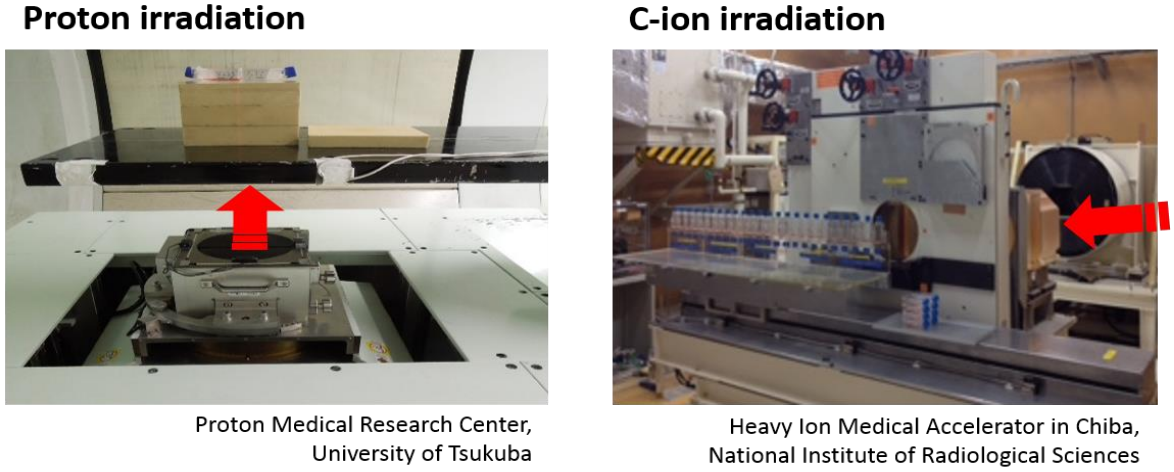

Figure 2.1. Proton and C-ion beam irradiation.

Photos of radiation procedure of protons and C-ions, at the PMRC, University of Tsukuba and at the HIMAC, NIRS. For proton beam irradiation, samples were placed on water-tough water and for C-ion irradiation, samples were installed proper case. The red arrows indicate a beam direction.

2.2.2 Irradiation conditions and selected doses:

Proton and carbon-beam irradiation was performed at a dose rate of approximately 3 Gy/min at the middle of the SOBP in a 10 cm × 10 cm field. The dose was adjusted according to specific parameters (e.g., temperature and atmospheric pressure) in each experiment. Each irradiation was performed at room temperature (25.5–26.0°C).

For clonogenic survival and chromosomal analyses, cells growing exponentially in T25 or T75 flasks and for detection of γ-H2A.X foci cells growing on glass coverslips in 6-well plates were placed at the middle of the proton and C-ion SOBPs and irradiated from the bottom (Figure 2.1; Figure 2.2 and Figure 2.3). Reference γ-ray irradiation was performed from both the top and bottom (Figure 2.4).

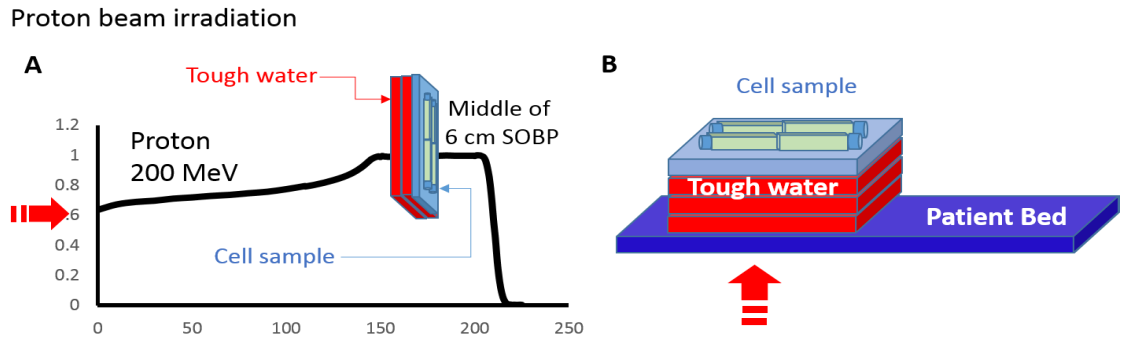

Figure 2.2. Simple illustration of Proton beam irradiation.

The dose distribution of 200 MeV proton beam is represented in panel A. For irradiation samples were placed directly on appropriate thick of tough-water materials to set the cells up at the middle of 6 cm spread out Bragg peak (SOBP). Simply depicted a sample placement in panel B. Red arrows indicate proton beams direction.

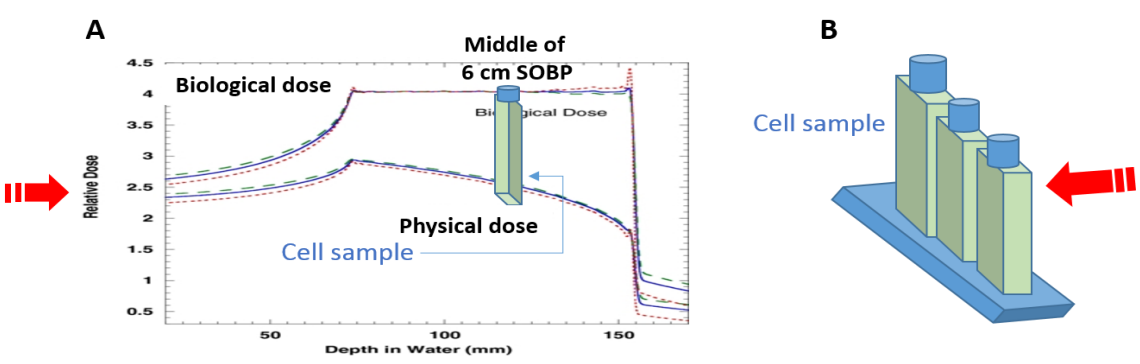

Figure 2.3. Simple illustration of C-ion beam irradiation

The dose distribution of 290 MeV/nucleon C-ions is represented in panel A. For irradiation samples were installed in proper case and samples were set up at the middle of 6 cm SOBP. Simply depicted a sample placement in panel B. Red arrows indicate beams direction and cell were attached arrow side layer of flask.

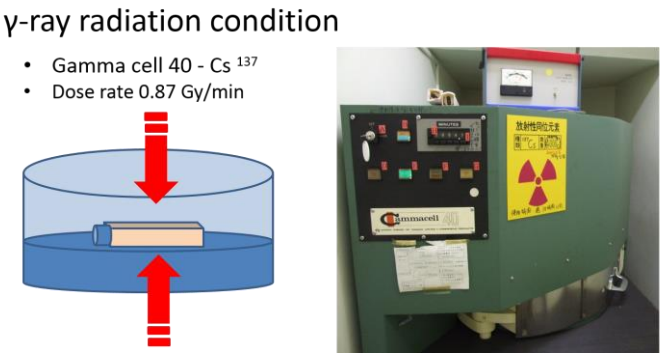

Figure 2.4. Simple illustration of γ-ray irradiation

For γ-ray irradiation samples were placed directly on tray and irraiated from both the top and bottom. Red arrows indicate irradiation direction.

The dose points selected for the wild-type cell colony formation assays were 0, 1, 2, 4, and 8 Gy, and those selected for the repair-deficient cell colony formation assays were 0, 0.5, 1, 2, and 4 Gy. In addition, the dose point selected for γ-H2A.X foci detection was 2 Gy because the standard dose per fraction in clinical practice is 2 Gy. As for chromosomal aberration, I selected 1 Gy to compare my results with other reports, since CHO and V79 cells are well studied with 1 Gy or less for chromosomal aberration (*31*).

2.3 Clonogenic survival assay

For the clonogenic survival assay, cells were seeded in T25 flasks at a density of 1×10^5 per flask 24 h prior to irradiation; exponentially growing cells were irradiated with either γ-rays, proton, or C-ion beams. Immediately after each irradiation, the cells were dispersed with 0.25% trypsin-EDTA and seeded onto 60-mm culture dishes at appropriate densities. The colonies were fixed and stained after 10 (wild-type cell lines) or 14 days (repair-deficient cell lines) of incubation. Five replicate dishes were seeded for each dose point, and colonies containing more than 50 cells were scored as survivors. See Figure 2.5 for detail. At least three independent experiments were performed.

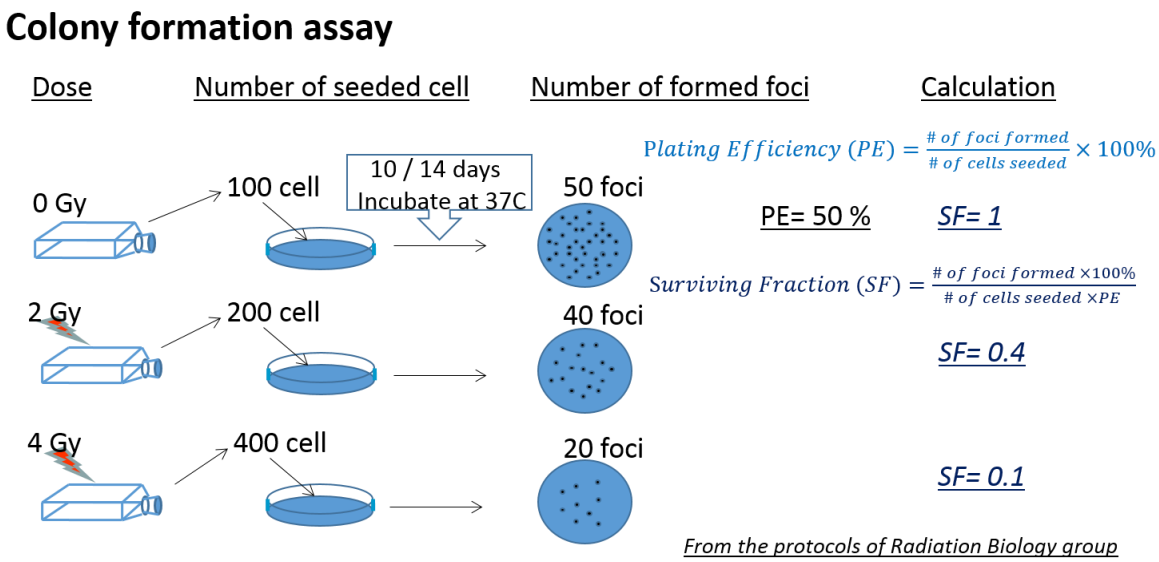

Figure 2.5. Simplified protocol for Colony formation assay

The resulting survival data were fitted according to the linear-quadratic (LQ) model using the GraphPad Prism software (GraphPad Software, Inc., San Diego, CA, USA). From these curves, the doses corresponding to 10% survival (D_{10}), $RBE_{0.1}$ values, survival fractions at 2 Gy (SF2), and α and β values were calculated and used to compare the effects of γ-rays, proton beams, and C-ion beams (Figure 2.6).

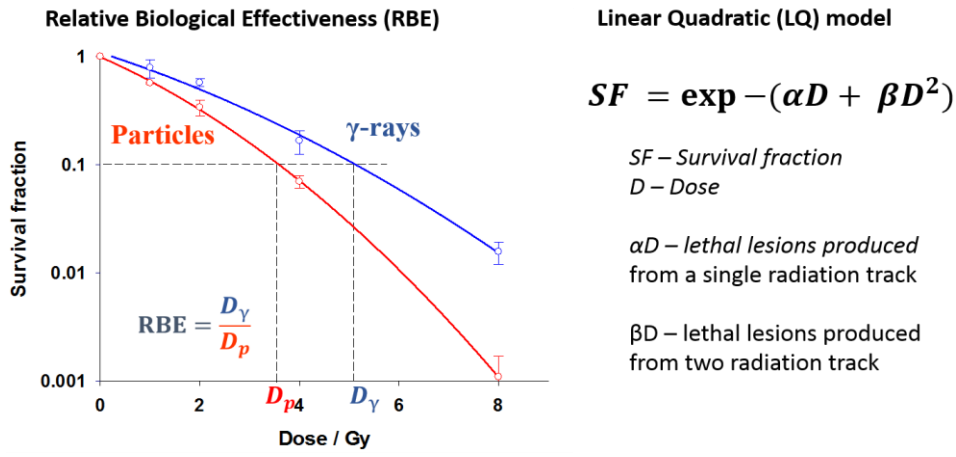

Figure 2.6. Simple description of RBE and LQ model

2.4 Immunocytochemical staining of γ-H2A.X

After each irradiation, the cells were fixed in 4% formaldehyde (Wako Pure Chemical Industries, Osaka, Japan) for 0.5, 3, 5, 7, 12, and 24 h.

The fixed cells were immunocytochemically stained with human monoclonal Anti-γphospho-Histone H2A.X (Ser139) Antibody (EMD Millipore, Darmstadt, Germany) according to the manufacturer's protocol with minor modifications. In brief, the fixed cells

were washed in PBS (-) and permeabilized in 0.5% Triton X-100 (Wako Pure Chemical Industries). Next, the cells were rinsed again in PBS (-) and blocked with 3% bovine serum albumin (Wako Pure Chemical Industries) in PBS (-) with 0.5% Tween-20 (Wako Pure Chemical Industries) for 30 min at room temperature in a humidified chamber. The cells were sequentially incubated for 1.5 h with a 1:1000 dilution of human monoclonal Anti-phospho-γ-Histone H2A.X (Ser139) antibody in blocking buffer and for 1 h with a 1:1000 dilution of Alexa Fluor 488-conjugated donkey anti-mouse immunoglobulin G (H+L) secondary antibody (Invitrogen/Molecular Probes, Eugene, Oregon, USA) in blocking buffer. The cells were subsequently counterstained with a 2-µg/mL solution of 4′,6-diamidino-2-phenylindole dihydrochloride n-hydrate (DAPI;Wako Pure Chemical Industries), and finally mounted with DAKO fluorescent mounting medium (DAKO North America, Carpinteria, CA,USA).

The resulting fluorescent images were captured using a fluorescence microscope (Biozero BZ-8000 KEYENCE; Tokyo, Japan), and the accompanying software was used to obtain Z-stacking images consisting of 4-6 images with 0.7 µm thickness in each nuclei to avoid possible overlapping of foci. From the obtained images, at least 50 nuclei per experiment and a total of more than 150 nuclei with distinct foci were selected for analysis. The number of foci was counted using "foci counter" software as previously described (*5*). Three independent experiments were performed.

2.5 Chromosome Aberration Analysis

To detect radiation-induced chromosome aberrations, colcemid (Irvine Scientific, Santa Ana, CA, USA) was added to the culture media at a final concentration of 0.1 µg/mL at 3 (a) and 16 h (b) after irradiation, after which the cells were incubated for an additional 4 h. It is known that under these conditions, cells harvested from (a) culture are mitotic cells arrested in the G2/M phase and cells harvested from (b) culture are in the second mitosis after release from the first G2/M arrest.

Following incubation with colcemid, the cells were trypsinized and incubated in a hypotonic (75mM) KCl solution. Next, the cells were fixed in a methanol:acetic acid (3:1) solution and air dried, and chromosome spreads were made as previously described (*32*). After Giemsa staining, the chromosomal aberrations were scored according to the conventions outlined by Savage (*33*). See Figure 2.7 for detail.

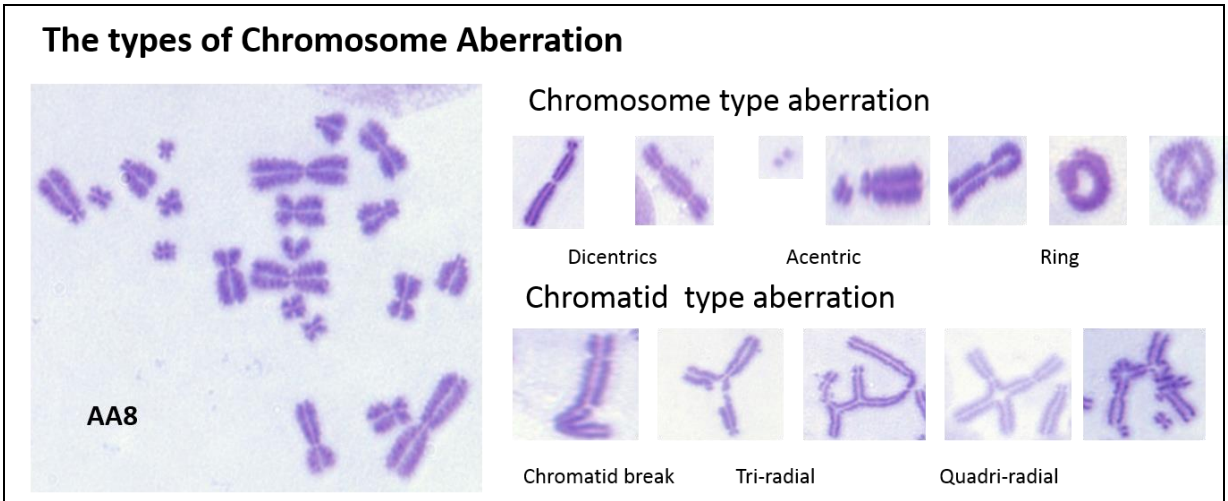

Figure 2.7. The classification of chromosome aberration

Variety of chromosome aberrations were observed after irradiation and scored according classification shown in above.

2.6 Statistical Analysis

The experimental values are expressed as means, and the error bars indicate the standard deviation (SD) calculated for each data point. Significant differences between data were assessed with Student's *t*-test. Probability (p) values of <0.05 were considered significant for all selected dose and time points. In addition, confidence interval estimation was performed for the colony survival assay, in which the RBE, α and β values were calculated.

3 Results

3.1 Colony formation assay

The results of the colony formation assays are shown in Figure 3.1.The mean survival data for each radiation treatment were fitted according to the LQ model.

Although shoulders were observed on the γ-rays and proton beam-induced survival curves for the wild-type V79 and AA8 cells and C-ion beam-induced survival curve of wild-type AA8 cell, these were not observed on the corresponding survival curves for the repair-deficient cell lines or C-ion beam-induced survival curves for wild-type V79 and repair deficient cell lines (Figure 3.1). However, as the calculated errors of the β-parameters were the same or higher than the mean value as shown in Table 1, the shape of the curves with the variable β-parameters may be inconsistent.

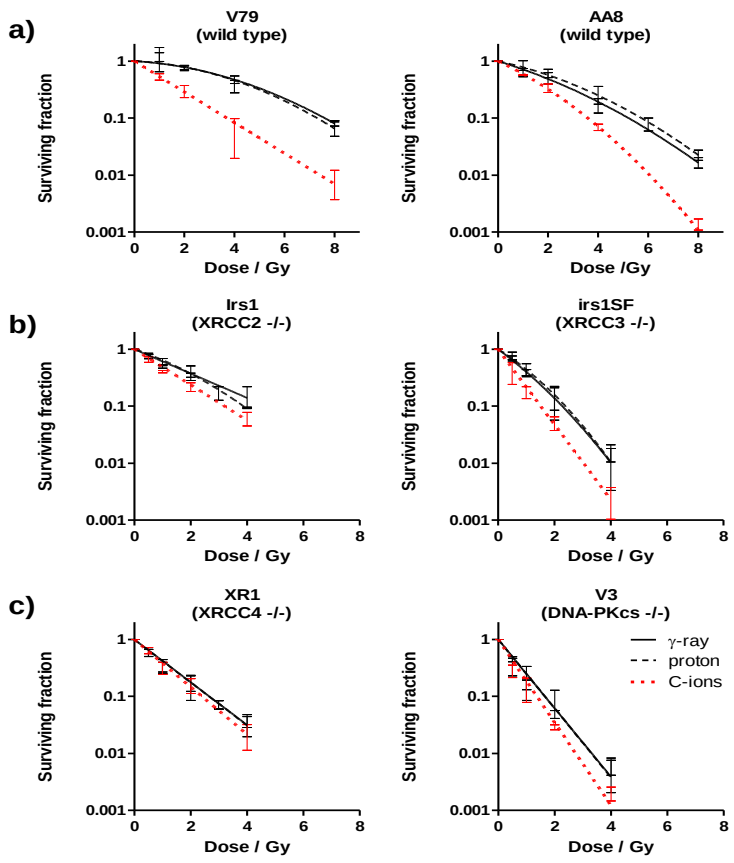

Figure 3.1. Survival curves in each cell line
Clonogenic survival curves are shown for Chinese hamster cell lines a) wild type V79 and AA8; b) HR-deficient irs1 and irs1SF; c) NHEJ deficient XR1 and V3 after irradiation with γ-rays or 200 MeV protons and 290 MeV C-ions. The curves were fitted by LQ model and the error bars represent SD.

The wild-type cells were most resistant, followed by the HR-deficient irs1 (XRCC2-/-), NHEJ-deficient XR1 (XRCC4-/-), HR-deficient irs1SF (XRCC3-/-), and NHEJ-deficient V3 cells (DNA-PKcs-/-) to all radiation types examined Figure 4.4). The cells responded to γ-rays and proton beams in a nearly identical manner; however, the wild-type and HR-deficient cell lines were more strongly sensitized to C-ions than were the NHEJ-deficient cell lines. In particular, the cytotoxic effect of C-ions on XR1 cells, which lack XRCC4, was smaller than that observed in the other cell lines (Figure 3.1; Figure 3.2)

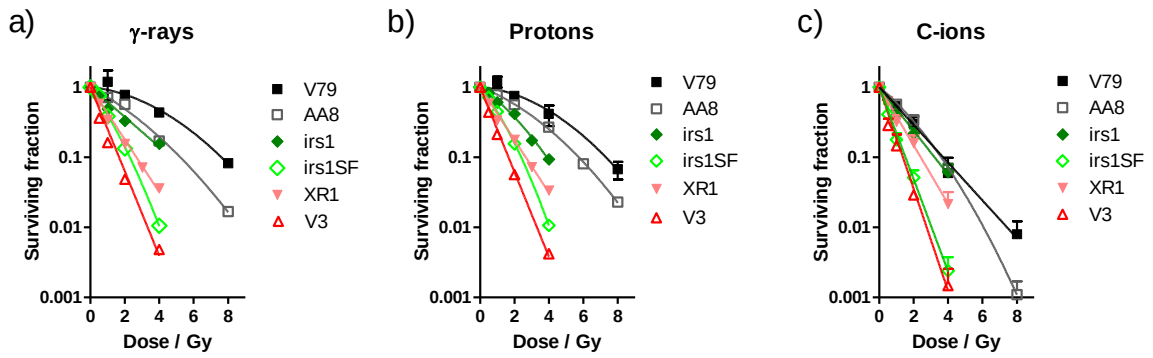

Figure 3.2. Survival curves in each radiation type
Clonogenic survival curves after γ-rays (a), protons (b) and C-ions (c) in the wild type (V79 and AA8); HR-deficient (irs1 and irs1SF); and NHEJ-deficient (XR1 and V3) cell lines.

As shown in Table 2.1 and Figure 3. 3 the RBE values at 10% survival ($RBE_{0.1}$) of protons to γ-rays ranged from 0.89 to 1.10, and no differences were observed among the wild-type, HR, and NHEJ-deficient cell lines. In contrast, the $RBE_{0.1}$ value of C-ions to γ-rays ranged from 1.07 to 2.10, and the $RBE_{0.1}$ values of the wild-type (2.10 ± 0.47 in V79; 1.37 ± 0.08 in AA8) and HR-deficient (1.40 ± 0.17 in irs1; 1.70 ± 0.41 in irs1SF) cell lines were significantly higher than those of the NHEJ-deficient cell lines (1.07 ± 0.33 in XR1; 1.11 ± 0.10 in V3). The 95% confidence intervals (CI) for the proton-beam $RBE_{0.1}$ values did not significantly exceed 1.00 in any of the examined cell lines. However, the 95% CIs of the C-ion $RBE_{0.1}$ values were significantly greater than 1.00 in the wild-type and HR-deficient cell lines but not in the NHEJ-deficient cell lines (Table 3.1). In addition, the α-values for each irradiation type, which were calculated according the LQ model, were plotted for each cell line (Figure 3.3). The α-values of the protons and γ-rays in the wild-type and HR-deficient cells (irs1) were lower or significantly lower than those in cells treated with C-ion beams. However, no differences were observed among the NHEJ-deficient cells with respect to the irradiation type. In contrast, the β-values did not differ with respect to the irradiation type in any of the cell lines (Table 3.1).

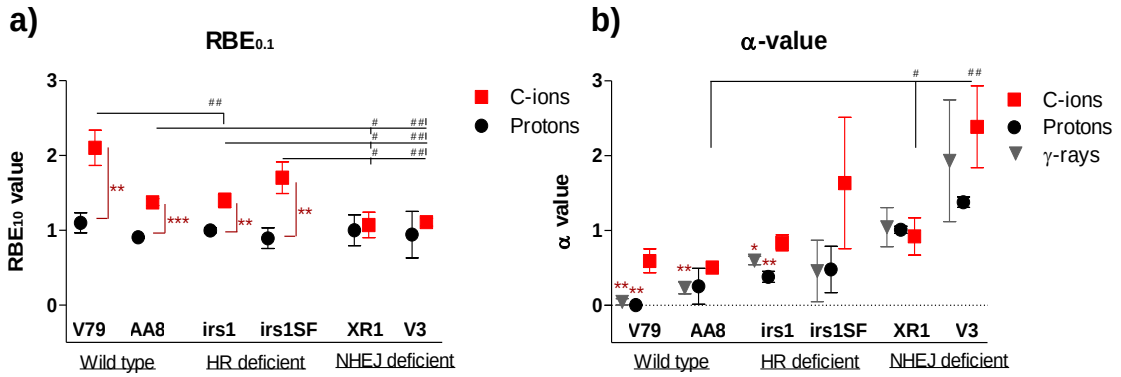

Figure 3.3. RBE and α-values of protons and C-ions.

Relative biological effectiveness values at 10 % ($RBE_{0.1}$) survival of protons and C-ions and α-values of all radiation types examined were calculated according LQ model. a) $RBE_{0.1}$ values of protons (●) and C-ion (■) in wild type V79 and AA8; HR-deficient irs1 and irs1SF; and NHEJ-deficient XR1 and V3 cell lines. b) α-values of γ-rays (▼), protons (●) and C-ions (■) in wild type V79 and AA8 cells, HR deficient irs1 and irs1SF, and NHEJ deficient XR1 and V3 cells. Student's *t*-test: ## $p < 0.01$, # $p<0.05$ – compared with wild type and HR-deficient cells; ** $p < 0.01$, * $p < 0.05$ compared with C-ions. The error bars represent SD.

Table 3.1 The parameters of Clonogenic survival assay

The α and β values and the percentage of surviving colonies after irradiation with a single dose of 2 Gy (SF2). D_{10} denotes a single dose of γ-rays, protons or C-ions that produces a 10% survival rate. $RBE_{0.1}$ indicates relative biological effectiveness calculated using isoeffective doses of γ-rays and protons or

Cell lines	IR types	α±95%CI(Gy^{-1})	β ± 95%CI (Gy^{-2})	SF2±95%CI	D_{10}±95%CI(Gy)	$RBE_{0.1}$±95%CI
Wild type	γ- rays	0.05±0.08	0.04±0.01	0.78±0.13	7.26±0.37	-
V79	protons	0.05±0.18	0.05±0.03	0.75±0.13	6.68±1.99	1.10±0.25
CH Lung Fibroblast	C-ions	0.59±0.31	0.02±0.06	0.30±0.13	3.49±0.94	2.10±0.47
	γ- rays	0.23±0.15	0.05±0.06	0.57±0.12	5.11±1.25	-
AA8	protons	0.25±0.46	0.03±0.07	0.56±0.31	5.64±1.45	0.91±0.02
CH Ovarian	C-ion	0.51±0.05	0.03±0.03	0.34±0.12	3.71±0.68	1.37±0.08
HR deficient	γ- rays	0.59±0.11	5.85e-014±1.02e-013	0.33±0.10	3.88±0.72	-
irs1 (XRCC2-/-)	protons	0.38±0.14	0.06±0.05	0.42±0.17	3.89±0.90	1.00±0.06
(sub-line of V79)	C-ions	0.84±0.20	3.07e-014±1.00e-013	0.22±0.08	2.78±0.65	1.40±0.17
	γ- rays	0.46±0.80	0.43±0.88	0.13±0.15	2.00±0.99	-
irs1SF (XRCC3-/-)	protons	0.48±0.61	0.35±0.92	0.15±0.14	2.29±1.31	0.89±0.27
(sub-line of AA8)	C-ions	1.63±1.72	0.27±0.92	0.05±0.02	1.17±0.31	1.70±0.41
NHEJ deficient	γ- rays	1.04±0.51	3.40e-004±1.15e-003	0.16±0.14	2.29±1.01	-
XR1 (XRCC4-/-)	protons	1.01±0.09	1.94e-012±6.58e-012	0.18±0.12	2.28±0.21	1.00±0.41
(sub-line of AA8)	C-ions	0.92±0.48	0.10±0.35	0.16±0.10	2.15±1.01	1.07±0.33
	γ- rays	1.93±1.59	0.18±0.63	0.05±0.04	1.11±0.47	-
V3 (DNA-PKcs-/-)	protons	1.38±0.13	0.34±0.94	0.06±0.13	1.40±0.92	0.94±0.61
(sub-line of AA8)	C-ions	2.39±1.07	5.34e-013±1.56e-012	0.03±0.006	1.00±0.04	1.11±0.10

C-ions at a 10% survival rate. A CI of 95% was calculated from 3 independent experiments.

3.2 Histone γ-H2A.X nuclear focus formation and dissolution

Cells were immunostained to detect phosphorylated histone at serine 139 (γ-H2A.X), and the resulting labeled foci were analyzed as DSB markers in the wild-type and repair-deficient cell lines following irradiation with 2 Gy γ-rays, protons, or C-ions. The cells were analyzed at 30 min and 3, 5, 7, 12, and 24 h after irradiation (Figure 3.4 and Figure 3.5).

The average number of foci per cell before irradiation (background) was 3.76 ± 1.04, and the background values were subtracted from each obtained data point. The number of foci peaked at 30 min (35.42 ± 4.66 after γ-rays; 36.90 ± 6.06 after protons; 29.86 ± 4.43 after C-ions) after irradiation and then decreased gradually over time up to the 24 h point in all examined cell lines.

The numbers foci per cell at 30 min were normalized to 100% to compare the repair kinetics according to the number of γ-H2A.X foci (Figure 3.4). The percentages of γ-H2A.X foci per cell did not significantly differ with respect to the three irradiation types in the wild-type cell AA8 or the HR-deficient cell line irs1 (Figure 3.4 –a, b); however, they were higher, but insignificant, in wild type V79 and significantly higher in the HR deficient irs1SF (XRCC3-/-) cell for up to 5 h after C-ion irradiation (Figure 3.4-a, b) as compared to protons. Furthermore, although the percentages of γ-H2A.X foci per cell in the NHEJ-deficient cell lines did not significantly differ between γ-rays and protons, C-ion beams induced a greater amount of γ-H2A.X foci especially at the early phase (Figure 3.4-c).

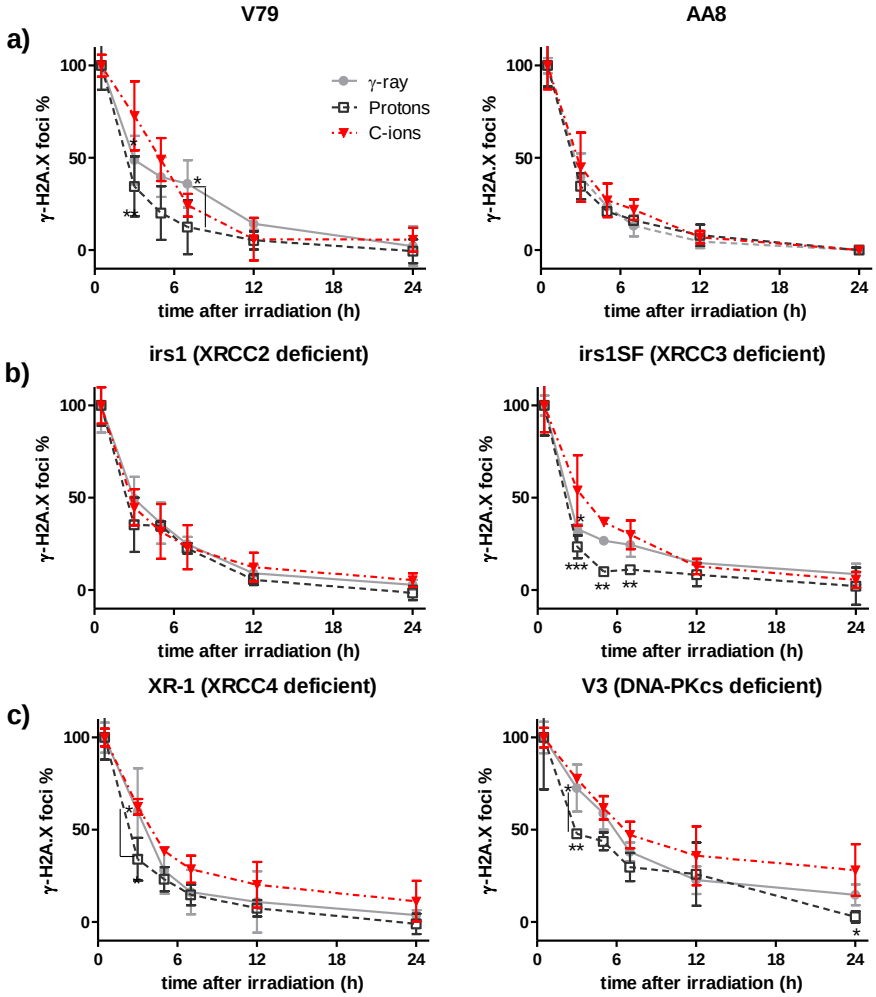

Figure 3.4. γ-H2A.X foci rejoining in each cell line

Time response of γ-H2A.X foci after irradiation with 2 Gy of γ-rays (●), protons (□) and C-ions (▼). The number of foci per cell was plotted after subtracting the number of foci in 0 Gy irradiated cell and the numbers at 30 min were normalized as 100 %. The γ-H2A.X foci formation and dissolution a) in wild type cell lines AA8 and V79; b) in HR deficient cell lines irs1 and irs1SF; and c) in NHEJ deficient cell lines XR1 and V3. Student's *t*-test: ** $p < 0.01$, * $p < 0.05$ compared with C-ion; Significant difference (p) between γ-rays and protons connected by line . The error bars represent SD.

When comparing the percentages of γ-H2A.X foci in the wild-type and HR- and NHEJ-deficient cell lines over time following each irradiation type, the percentages of foci decreased almost in the same manner in all cell lines, except for the NHEJ-deficient V3 (DNA-PKcs-/-) line after irradiation with γ-rays, protons, and C-ions (Figure 3.5).

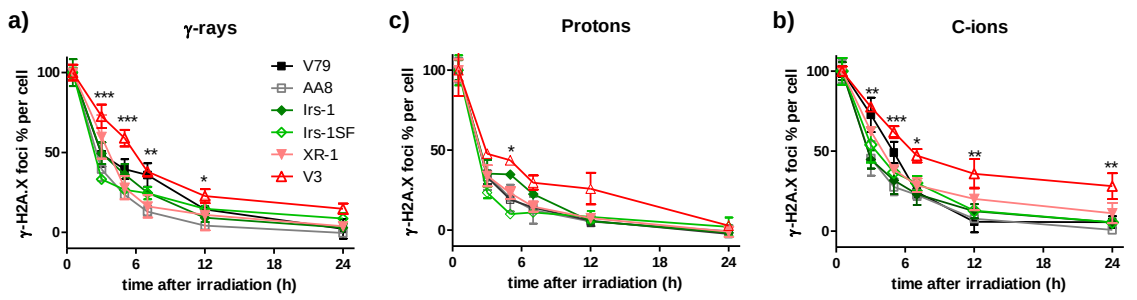

Figure 3.5. Formation and dissolution of γ-H2A.X foci after each radiation type
The γ-H2A.X foci rejoining after γ-rays (a), protons (b) and C-ions (c) in the wild type (V79 and AA8); HR-deficient (irs1 and irs1SF); and NHEJ-deficient (XR1 and V3) cell lines. Student's *t*-test: ** $p < 0.01$, * $p < 0.05$ compared with wild type cell lines (V3 vs AA8). The error bars represent SD.

3.3 Radiation-induced chromosomal aberrations

The wild-type (V79, AA8), HR- (irs1, irs1SF), and NHEJ-deficient (XR1, V3) cell lines were scored for various chromosomal aberrations induced by γ-ray, proton, and C-ion radiation. After each irradiation, colcemid was added at 3 and 16 h and incubated for an additional 4 h before fixation. The numbers of chromosomal aberrations in un-irradiated cells were subtracted from those obtained at each time point. Following irradiation, the total number of chromosomal aberrations was significantly higher in the repair-deficient cells than in the wild-type cells (Figure 3.6). I compared the chromosomal aberrations at early (3 h) and late (16 h) time points after irradiation in all cell lines and found a tendency towards an increase in aberrations at later time points in some cells, although no significant differences were observed (Figure 3.6).

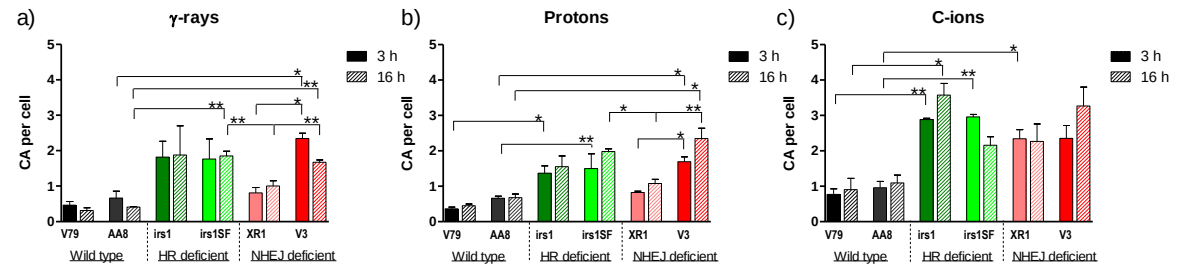

Figure 3.6. The incidence of chromosome aberration after radiations

Chromosome aberrations induced by 1 Gy of γ-rays (a), protons (b) and C-ions (c) after 3 hours (filled column) and 16 hours (gradient column) irradiations were plotted in the wild type (V79 and AA8); HR-deficient (irs1 and irs1SF); and NHEJ-deficient (XR1 and V3) cell lines after subtracting the number of 0 Gy-irradiated cells. Student's *t*-test: ** $p < 0.01$, * $p < 0.05$. The error bars represent SD.

The incidence of chromosomal aberration was higher after C-ion-beam irradiation than after the other radiation types; in particular, chromatid-type aberrations tended to increase in response to C-ion beams (Figure 3.6). Furthermore, both chromosome and chromatid types aberration were significantly higher in repair-deficient cells than in wild-type cells. The occurrences of chromosome and chromatid type aberrations did not significantly differ with respect to radiation types in any cell line (Figure 3.7).

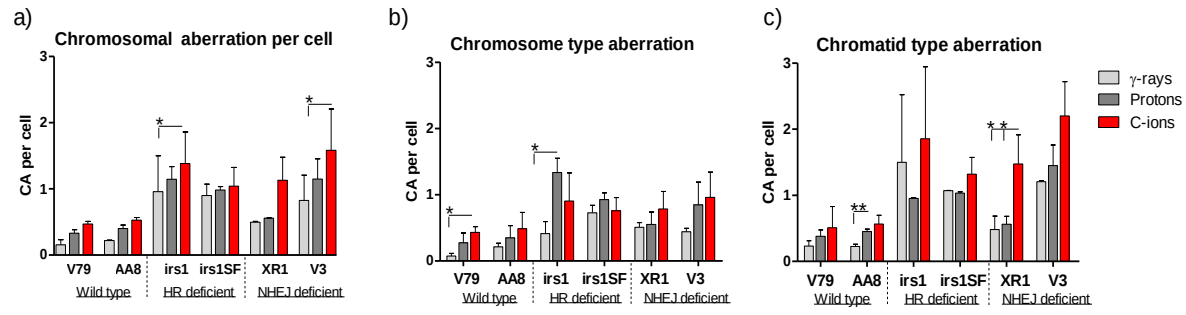

Figure 3.7. Total cromosome aberration; chromsome type and chromatid type aberrations (16 h after irradiation)

The incidence of total chromosome aberration (a), chromosome type aberration (b) and chromatid type aberrations (c) after 1 Gy of γ-rays (light gray column), protons (dark gray column), and C-ions (red column). Student's *t*-test: * $p < 0.05$. The error bars represent SD.

The types of aberrations observed in the repair-deficient cells are shown in Figure 3.8. Since there were no significant differences in types of chromosome aberration between early (3 h) and late (16 h) time points, only the results at 16 h were shown in Figure 3.7 and Figure 3.8. The occurrences of chromosome type and chromatid type aberrations did not significantly differ with respect to radiation types in any cell line. Regarding the chromatid type

aberrations, breaks and tri-radial types were more frequent in the HR- and NHEJ-deficient cells than in the wild-type cells (Figure 3.8-B). Among the repair deficient cells, NHEJ deficient XR1 (XRCC4-/-) cells showed significantly smaller numbers of chromatid type aberrations, chromatid type-breaks and tri-radial types than other repair deficient cell lines. Chromatid type-breaks occurred more frequently than other types of aberrations in all cell lines in all irradiation types. In addition, regarding the chromosome type aberrations, the ring with tail was more frequent in the NHEJ-deficient cells, and breaks were more frequent in both HR- and NHEJ-deficient cells than in wild-type cells (Figure 3.8-A).

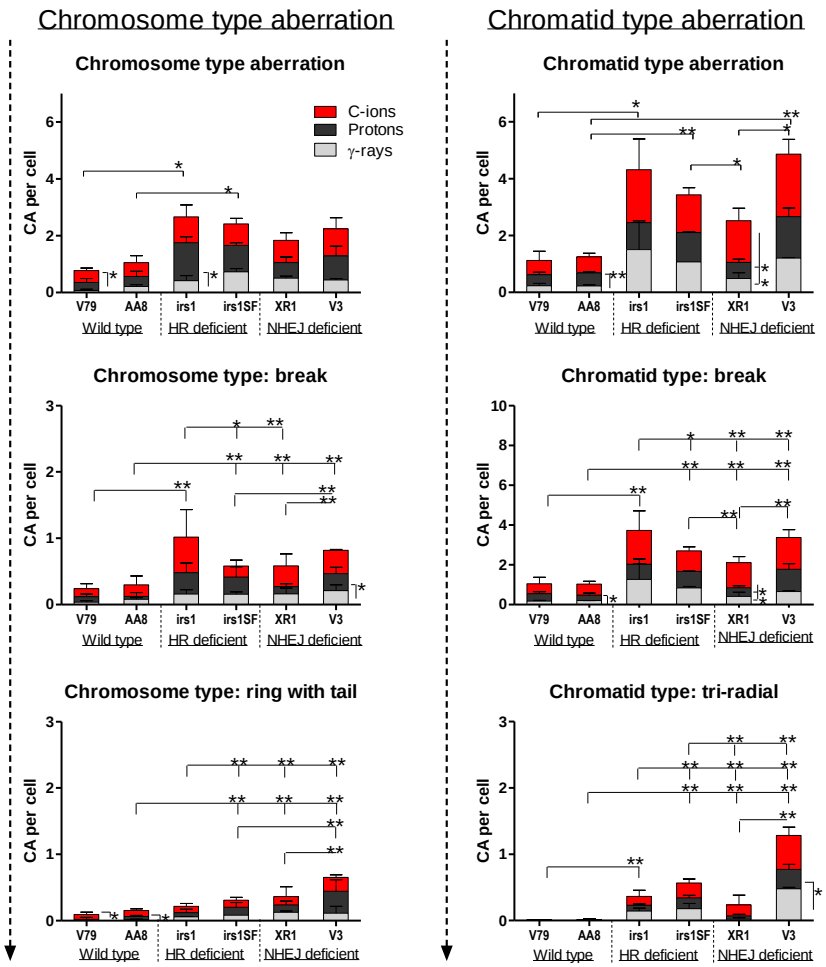

Figure 3.8. Frequently observed chromosome aberrations (16 h after irradiation)

A) The number of chromosome type aberrations and frequently occurred chromosome type: break and ring with tail type aberrations per cell were plotted in each cell lines after irradiation with γ-rays (light gray), protons (dark gray) and C-ions (black). B) The number of chromatid type aberrations and more frequently occurred chromatid type: break and tri-radial type aberrations per cell were plotted in each cell lines after irradiation with γ-rays (light gray), protons (dark gray) and C-ions (red). Student's *t*-test: ** $p < 0.01$, * $p < 0.05$. The error bars represent SD.

4 Discussion

Studies of how the NHEJ and HR pathways contribute to the repair of DSBs induced by different types of radiation are essential not only to understand the responses of cancers to different radiotherapy types but also to developing molecular targeting radiosensitizing therapies that incorporate different particle beams.

The choice of DSBs repair pathways is a complex process that depends on many factors, including the DSBs induction process (*19, 34*), repair protein proficiencies (*10, 35*), cell cycle phase (*14, 15*), and cell cycle checkpoint control (*13, 36*). Many pathways have evolved to resolve DSBs; these include not only the major NHEJ and HR pathways but also the alternative end-joining pathway, microhomology-mediated end-joining, synthesis-dependent strand annealing and single-strand annealing, and when one DSBs repair pathway fails, others are activated (*10, 11, 14*). The occurrence and quality of radiation-induced DSBs are known to depend on the ionization density associated with the radiation (*19, 34, 37*), which should exert a significant influence on the subsequent repair pathway choice. Therefore, in the present study I compared the contributions of the NHEJ and HR pathways in DSB repair in genetically established the NHEJ- or HR-deficient cells following γ-ray, proton, and C-ion irradiation.

NHEJ is a simple, rapid, and efficient repair pathway that works throughout the cell cycle (*14, 15, 38*). See Figure 1.3 for detail. DNA-PKcs is known to play a key role in this repair pathway and the phosphorylation status of DNA-PKcs itself indicates the level of kinase activity and the DNA end-binding ability, which probably determines the choice between the NHEJ and HR pathways (*35, 36*). In this study, I used two different NHEJ-deficient cell lines, V3 (DNA-PKcs-/-) and XR1 (XRCC4-/-), and my survival results showed that V3 was most sensitive to all radiation types (Figure 3.1-c; Figure 3.2).

The other NHEJ-deficient cell line, XR1, lacks the functional XRCC4 protein, which is known to play an important role in the ligation of broken ends via DNA ligase IV and XLF (*39*). In addition, XRCC4 is known to assist the recruitment of NHEJ-dependent DNA end-processing enzymes to the DSBs in order to facilitate the repairs of specific breaks (*40*). However, XR1 cells exhibited less sensitivity to all radiation types when compared with V3 cells (Figure 3.1-c, Figure 3.2). This difference could indicate that although XRCC4 lack may induce incomplete NHEJ, this mutation is not as lethal as DNA-PKcs lack. Furthermore,

other repair pathways may compensate for XRCC4 deficiency (*10*), whereas DNA-PKcs deficiency cannot be rescued. These findings are compatible with other reports in which DNA-PKcs was suggested to be the major protein involved in the repair pathway direction or selection (*35*, *41*).

The HR-defective cell lines irs1 (XRCC2-/-) and irs1SF (XRCC3-/-) exhibited higher levels of sensitivity to all radiation types when compared with the wild-type cells (Figure 3.1-b; Figure 3.2). XRCC2 and XRCC3 are paralogs of RAD51 that exist in two distinct complexes: one comprises RAD51B, RAD51C, RAD51D, and XRCC2 (BCDX2) and the other comprises RAD51C and XRCC3 (CX3) (*42*, *43*). The BCDX2 complex preferentially binds ssDNA and acts during the pre-synaptic phase of HR (*43*); the CX3 complex plays an essential role in the resolution of Holliday junctions created during HR (*42*). From my survival results, XRCC3-/- irs1SF cells were 1.9, 1.7, and 2.4-fold more sensitive than XRCC2-/- irs1 cells in response to γ-ray, proton, and C-ion irradiation, respectively. Therefore, my results could indicate that the contribution of XRCC3 is greater than XRCC2 in repair of DNA damages after all radiation types, in particular, its contribution is greater following C-ion radiation than other types of radiation.

As shown in the Figure 3.3 and Table 3.1, the proton $RBE_{0.1}$values in the wild-type and NHEJ- and HR-deficient cells ranged from 0.89 to 1.11 and did not significantly differ. In contrast, the C-ion $RBE_{0.1}$values in the NHEJ-deficient cells were significantly lower than those in the HR-deficient or wild-type cells. Furthermore, the C-ion and proton $RBE_{0.1}$values were nearly the same in the NHEJ-deficient cells, whereas the C-ion values were significantly higher than the proton values in the wild-type and HR-deficient cells. As a result, the cytotoxicity ratios of C-ions to protons were 10%–20% higher in the NHEJ-deficient cells and 40%–90% higher in the wild-type and HR-deficient cells. This could indicate that the repair of C-ion-induced DSBs requires a greater contribution from the HR pathway than to DSBs resulting from γ-ray or proton irradiation.

Furthermore, I compared the α-values calculated according to the LQ model, which determines low-dose (up to 5 Gy) sensitivity and represents the contributions of single-event damage (*44*). The α-values for C-ions were significantly higher than those for γ-rays and protons in both the wild-type and HR-deficient cell lines. However, these values did not significantly differ in the NHEJ-deficient cells with respect to the radiation types (Figure 3.3). In addition, α-values of NHEJ-deficient cells were significantly higher than wild-type cells while HR deficient cells were not. These findings indicate that C-ion beams should induce a

greater amount of single-track DSBs than protons or γ-rays “at the same dose”. This difference can be explained by the track structure of these types of irradiation; C-ions have high-density ionizing cores that yield more single-track DSBs than sparsely ionizing protons or γ-rays (*45, 46*). However, clinical C-ion beams are not absolutely pure, i.e. contamination by low LET components due to fragmentation of the primary ions cannot be avoided (*46*), and the low LET components including delta ray ionization probably induce double-track DSBs at the penumbra region (*45*).

In all cell lines, the number of γ-H2A.X foci at 30 min after C-ion irradiation was lower than that after proton and γ-ray irradiation, indicating that the number of DSBs is lower in response to the same dose of high LET C-ion irradiation (Figure 4.1). However, my results indicated that the number of residual foci at 12 and 24 h after irradiation was higher in the NHEJ-deficient V3 and XR1 cells than in the wild-type and HR-deficient cells after C-ion irradiation. It may indicates that C-ion-induced DSBs are more irreparable than DSBs induced by γ-rays and protons. In particular, the residual fraction of γ-H2A.X foci was significantly higher in the NHEJ-deficient V3 cells from 3 to 7 h after all types of irradiation than other cell lines (Figure 3.4; Figure 3.5), that is compatible with the clonogenic survival data indicated in Figure 3.2. Mao et al. reported that the NHEJ pathway occurred within 30 min, whereas the HR pathway required a much longer time (≥7 h), and that the efficiency of NHEJ was three-fold higher than that of HR in actively cycling cells (*38*). In addition, the residual or persistent γ-H2A.X foci at later time points may represents the chromatin alteration rather than un-repaired DSBs, and chromatin alterations are more likely to occur at heterochromatic regions repaired with slow kinetics (*47*). Therefore, the residual foci observed at later time points may indicate the occurrence of HR, and the HR pathway was found to have a greater role in C-ion-induced DSB repair. Furthermore, regarding radiation-induced cell cycle arrest in the G2/M phase, my results showed that C-ion beams delayed cell cycle arrest and might have thus provided sufficient time for HR pathway-mediated repair (data not shown).

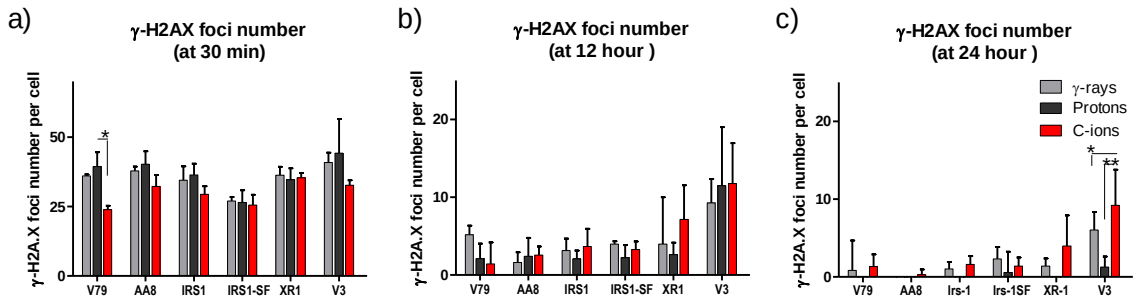

Figure 4.1. γ-H2A.X foci number at different time points after irradiation

The γ-H2A.X foci number per nucleus at 30 min (a), 12 hour (b), and 24 hour (c) after irradiation with 2 Gy γ-rays (light gray), protons (dark gray), and C-ions (red). Student's *t*-test: ** $p < 0.01$, * $p < 0.05$ between radiation types. The error bars represent SD.

The chromosomal aberrations after irradiation with 1Gy γ-rays, protons, and C-ion beams were significantly higher in both the NHEJ (XR1 and V3) and HR-deficient (irs1 and irs1SF) cells relative to the wild-type cells in response to all radiation types (Figure 3.6; Figure 3.7). The high aberration levels in the HR-deficient cells might result from the increased rate of DSB repair via the error-prone NHEJ pathway in the HR-deficient cells. Furthermore, the differences in aberration levels between the NHEJ-deficient XR1 and V3 cell lines after irradiation with γ-rays and protons (Figure 3.7) could be explained as follows: error-free HR compensated for NHEJ impairment due to the loss of XRCC4 (XR1) but not DNA-PKcs (V3). However, definitive reasons to explain these observations remain unidentified. Overall, the chromosomal aberration level did not significantly differ in response of γ-rays and protons, whereas C-ion irradiation induced increased aberration levels in all cell lines (Figure 3.7-a). It may indicate that although both NHEJ and HR pathways are essential, C-ion induced DNA damage is not easy to be repaired correctly.

Recently, Grosse et al. compared the cytotoxicities of photons and protons in the same cell lines and reported that proton-induced DSBs preferentially require the HR repair pathway (*48*). However, I did not observe a significant difference following γ-ray and proton irradiation. This discrepancy was likely due to differences in the colony formation assay method. Grosse et al. incubated irradiated cells for 20 hours before seeding. Barendsen mentioned that single-track damage was not repaired by delayed plating and that single-track lethal damage encompassed two types of damage wherein one component is not repaired by delayed plating and is very strongly dependent on LET and the other component comprises potentially lethal damage that is weakly dependent on LET Thus, Gross et al. might have evaluated the contributions of HR and NHEJ to the repair of single-event type damage that could not be repaired by delayed plating (*44*, *49*). In contrast, my colony formation results

represent all types of damage that lead to reproductive death, including single-event type, sub-lethal, and potentially lethal damage, suggesting that the NHEJ pathway plays a greater role than the HR pathway in DNA damage repair caused not only by γ-rays but also by protons. In addition, γ-ray-induced DSB rejoining is strictly dependent on the NHEJ repair system integrity and the NHEJ plays a more important role in repair after C-ions (*14*, *50*). My results are compatible with that earlier reports and suggest that NHEJ is the major pathway and that, among many factors, DNA-PKcs plays the most important role in regulating the process of repairing DSBs induced by protons as well as γ-rays.

In conclusion, the DNA-PKcs-dependent NHEJ pathway plays an important role in repairing DSBs induced by both clinical proton and C-ion beams. Furthermore, my results suggest that the HR pathway is more involved in the repair of DSBs induced by C-ion beams than those induced by proton beams or γ-rays.

5 Acknowledgements

I wish to express my deep gratitude to my supervisor Professor Koji Tsuboi for his scientific guidance, support, discussions and encouragement throughout this work.

I am deeply indebted to Professor David J Chen and Asaithamby Aroumougame for their invaluable suggestions and technical assistance; and for the kind hospitality during my research work in Radiation Biology Department at University of Texas Southwestern Medical Center.

I am deeply indebted to Professor Takeji Sakae for their invaluable suggestions and technical assistance in proton beams irradiation.

I would like to thank Mr. Ryoichi Hirayama and members of HIMAC facility at National Institute of Radiological Sciences to their support and help in my experiment.

I am grateful to assistant professor Kenshi Suzuki and my lab-members Mr. Lue Sun, Mr. Ito Kazuya, Mr. Takaaki Ishikawa, Ms. Eri Manabe (she is very kind and friendly one and without her assistance it was tough to complete my PhD work on time) and Ms. Eri Hiratsuka for their support and help on the experiment. I also wish to thank Ms. Yoko Mori and Ms. Junko Zenkoh for their kind help and support all experiment procedure.

I would like to thank to the Seiwa and Atsumi Foundation for Inbound Students for providing the scholarship.

I specially thank my family, my husband, my father, and brother. Without their support and care, these past several years have not been an easy to ride, both academically and personally.

5.1 Declaration of interest:

This work was partly supported by a Grant-in-Aid (24390287) from the Ministry of Education, Culture, Sports, Science & Technology of Japan; and National Aeronautics and Space Association (NNX13AD57G to AA and DJC). The part of this work was approved and performed under the Research Project with Heavy Ions at NIRS-HIMAC.

6 References

1. Ando K, Koike S, Kawachi K, Hiraoka T, Ohara H, Yokota M, et al. Relative biological effectiveness of the therapeutic proton beams at NIRS and Tsukuba University. Nihon Igaku Hoshasen Gakkai Zasshi. 1985; 45:531-5.
2. Belli M, Cera F, Cherubini R, Haque AM, Ianzini F, Moschini G, et al. Inactivation and mutation induction in V79 cells by low energy protons: re-evaluation of the results at the LNL facility. Int J Radiat Biol. 1993; 63:331-7.
3. Di Pietro C, Piro S, Tabbi G, Ragusa M, Di Pietro V, Zimmitti V, et al. Cellular and molecular effects of protons: Apoptosis induction and potential implications for cancer therapy. Apoptosis. 2006; 11:57-66.
4. Gerelchuluun A, Hong Z, Sun L, Suzuki K, Terunuma T, Yasuoka K, et al. Induction of in situ DNA double-strand breaks and apoptosis by 200 MeV protons and 10 MV X-rays in human tumour cell lines. Int J Radiat Biol. 2011; 87:57-70.
5. Hong Z, Kase Y, Moritake T, Gerelchuluun A, Sun L, Suzuki K, et al. Lineal energy-based evaluation of oxidative DNA damage induced by proton beams and X-rays. Int J Radiat Biol. 2013; 89:36-43.
6. Kagawa K, Murakami M, Hishikawa Y, Abe M, Akagi T, Yanou T, et al. Preclinical biological assessment of proton and carbon ion beams at Hyogo Ion Beam Medical Center. Int J Radiat Oncol Biol Phys. 2002; 54:928-38.
7. Koike S, Ando K, Oohira C, Fukawa T, Lee R, Takai N, et al. Relative biological effectiveness of 290 MeV/u carbon ions for the growth delay of a radioresistant murine fibrosarcoma. J Radiat Res. 2002; 43:247-55.
8. Davis AJ, Chen BP, Chen DJ. DNA-PK: a dynamic enzyme in a versatile DSB repair pathway. DNA Repair (Amst). 2014; 17:21-9.
9. Langerak P, Mejia-Ramirez E, Limbo O, Russell P. Release of Ku and MRN from DNA ends by Mre11 nuclease activity and Ctp1 is required for homologous recombination repair of double-strand breaks. PLoS Genet. 2011; 7:e1002271.
10. Pierce AJ, Hu P, Han M, Ellis N, Jasin M. Ku DNA end-binding protein modulates homologous repair of double-strand breaks in mammalian cells. Genes Dev. 2001; 15:3237-42.
11. Reynolds P, Anderson JA, Harper JV, Hill MA, Botchway SW, Parker AW, et al. The dynamics of Ku70/80 and DNA-PKcs at DSBs induced by ionizing radiation is dependent on the complexity of damage. Nucleic Acids Research. 2012; 40:10821-31.
12. Krejci L, Altmannova V, Spirek M, Zhao X. Homologous recombination and its regulation. Nucleic Acids Res. 2012; 40:5795-818.

13. Mao Z, Bozzella M, Seluanov A, Gorbunova V. DNA repair by nonhomologous end joining and homologous recombination during cell cycle in human cells. Cell Cycle. 2008; 7:2902-6.
14. Bee L, Fabris S, Cherubini R, Mognato M, Celotti L. The efficiency of homologous recombination and non-homologous end joining systems in repairing double-strand breaks during cell cycle progression. PLoS One. 2013; 8:e69061.
15. Rothkamm K, Kruger I, Thompson LH, Lobrich M. Pathways of DNA double-strand break repair during the mammalian cell cycle. Mol Cell Biol. 2003; 23:5706-15.
16. Whitmore GF, Varghese AJ, Gulyas S. Cell cycle responses of two X-ray sensitive mutants defective in DNA repair. Int J Radiat Biol. 1989; 56:657-65.
17. Yajima H, Fujisawa H, Nakajima NI, Hirakawa H, Jeggo PA, Okayasu R, et al. The complexity of DNA double strand breaks is a critical factor enhancing end-resection. DNA Repair. 2013; 12:936-46.
18. Asaithamby A, Chen DJ. Mechanism of cluster DNA damage repair in response to high-atomic number and energy particles radiation. Mutat Res. 2011; 711:87-99.
19. Hada M, Sutherland BM. Spectrum of complex DNA damages depends on the incident radiation. Radiat Res. 2006; 165:223-30.
20. Wang H, Wang X, Zhang P, Wang Y. The Ku-dependent non-homologous end-joining but not other repair pathway is inhibited by high linear energy transfer ionizing radiation. DNA Repair (Amst). 2008; 7:725-33.
21. Fuller LF, Painter RB. A Chinese hamster ovary cell line hypersensitive to ionizing radiation and deficient in repair replication. Mutat Res. 1988; 193:109-21.
22. Chu EH, Brimer P, Jacobson KB, Merriam EV. Mammalian cell genetics. I. Selection and characterization of mutations auxotrophic for L-glutamine or resistant to 8-azaguanine in Chinese hamster cells in vitro. Genetics. 1969; 62:359-77.
23. Sakaguchi DS, Moeller JF, Coffman CR, Gallenson N, Harris WA. Growth cone interactions with a glial cell line from embryonic Xenopus retina. Dev Biol. 1989; 134:158-74.
24. Tebbs RS, Zhao Y, Tucker JD, Scheerer JB, Siciliano MJ, Hwang M, et al. Correction of chromosomal instability and sensitivity to diverse mutagens by a cloned cDNA of the XRCC3 DNA repair gene. Proc Natl Acad Sci U S A. 1995; 92:6354-8.
25. Jones NJ, Cox R, Thacker J. Isolation and cross-sensitivity of X-ray-sensitive mutants of V79-4 hamster cells. Mutat Res. 1987; 183:279-86.
26. Nohtomi A, Sakae T, Tsunashima Y, Kohno R. Dosimetry of pulsed clinical proton beams by a small ionization chamber. Medical Physics. 2001; 28:1431-5.
27. Wilkens JJ, Oelfke U. Analytical linear energy transfer calculations for proton therapy. Medical Physics. 2003; 30:806-15.
28. Deasy J. ICRU report 49, Stopping Powers and Ranges for Protons and Alpha Particles. International Commission on Radiation Units and Measurements. 1993.

29. Fukumura A, Hiraoka T, Omata K, Takeshita M, Kawachi K, Kanai T, et al. Carbon beam dosimetry intercomparison at HIMAC. Physics in Medicine and Biology. 1998; 43:3459-63.

30. Kanai T, Endo M, Minohara S, Miyahara N, Koyama-ito H, Tomura H, et al. Biophysical characteristics of HIMAC clinical irradiation system for heavy-ion radiation therapy. Int J Radiat Oncol Biol Phys. 1999; 44:201-10.

31. Nagasawa H, Brogan JR, Peng Y, Little JB, Bedford JS. Some unsolved problems and unresolved issues in radiation cytogenetics: a review and new data on roles of homologous recombination and non-homologous end joining. Mutat Res. 2010; 701:12-22.

32. Cornforth MN, Bedford JS. X-Ray-Induced Breakage and Rejoining of Human Interphase Chromosomes. Science. 1983; 222:1141-3.

33. Savage JRK. Classification and Relationships of Induced Chromosomal Structural-Changes. Journal of Medical Genetics. 1976; 13:103-22.

34. Belli M, Cherubini R, Dalla Vecchia M, Dini V, Esposito G, Moschini G, et al. DNA fragmentation in mammalian cells exposed to various light ions. Adv Space Res. 2001; 27:393-9.

35. Neal JA, Dang V, Douglas P, Wold MS, Lees-Miller SP, Meek K. Inhibition of homologous recombination by DNA-dependent protein kinase requires kinase activity, is titratable, and is modulated by autophosphorylation. Mol Cell Biol. 2011; 31:1719-33.

36. Shrivastav M, Miller CA, De Haro LP, Durant ST, Chen BP, Chen DJ, et al. DNA-PKcs and ATM co-regulate DNA double-strand break repair. DNA Repair (Amst). 2009; 8:920-9.

37. Eccles LJ, O'Neill P, Lomax ME. Delayed repair of radiation induced clustered DNA damage: friend or foe? Mutat Res. 2011; 711:134-41.

38. Mao Z, Bozzella M, Seluanov A, Gorbunova V. Comparison of nonhomologous end joining and homologous recombination in human cells. DNA Repair (Amst). 2008; 7:1765-71.

39. Grawunder U, Wilm M, Wu XT, Kulesza P, Wilson TE, Mann M, et al. Activity of DNA ligase IV stimulated by complex formation with XRCC4 protein in mammalian cells. Nature. 1997; 388:492-5.

40. Kusumoto R, Dawut L, Marchetti C, Lee JW, Vindigni A, Ramsden D, et al. Werner protein cooperates with the XRCC4-DNA ligase IV complex in end-processing. Biochemistry. 2008; 47:7548-56.

41. Hammel M, Yu Y, Mahaney BL, Cai B, Ye R, Phipps BM, et al. Ku and DNA-dependent protein kinase dynamic conformations and assembly regulate DNA binding and the initial non-homologous end joining complex. J Biol Chem. 2010; 285:1414-23.

42. Liu Y, Tarsounas M, O'Regan P, West SC. Role of RAD51C and XRCC3 in genetic recombination and DNA repair. J Biol Chem. 2007; 282:1973-9.

43. Masson JY, Tarsounas MC, Stasiak AZ, Stasiak A, Shah R, McIlwraith MJ, et al. Identification and purification of two distinct complexes containing the five RAD51 paralogs. Genes Dev. 2001; 15:3296-307.

44. Franken NAP, Oei AL, Kok HP, Rodermond HM, Sminia P, Crezee J, et al. Cell survival and radiosensitisation: Modulation of the linear and quadratic parameters of the LQ model (Review). International Journal of Oncology. 2013; 42:1501-15.

45. Nakajima NI, Brunton H, Watanabe R, Shrikhande A, Hirayama R, Matsufuji N, et al. Visualisation of gamma H2AX Foci Caused by Heavy Ion Particle Traversal; Distinction between Core Track versus Non-Track Damage. Plos One. 2013; 8.

46. Hirayama R, Ito A, Tomita M, Tsukada T, Yatagai F, Noguchi M, et al. Contributions of direct and indirect actions in cell killing by high-LET radiations. Radiat Res. 2009; 171:212-8.

47. Costes SV, Chiolo I, Pluth JM, Barcellos-Hoff MH, Jakob B. Spatiotemporal characterization of ionizing radiation induced DNA damage foci and their relation to chromatin organization. Mutat Res. 2010; 704:78-87.

48. Grosse N, Fontana AO, Hug EB, Lomax A, Coray A, Augsburger M, et al. Deficiency in homologous recombination renders Mammalian cells more sensitive to proton versus photon irradiation. Int J Radiat Oncol Biol Phys. 2014; 88:175-81.

49. Barendsen GW. The Relationships between Rbe and Let for Different Types of Lethal Damage in Mammalian-Cells - Biophysical and Molecular Mechanisms. Radiation Research. 1994; 139:257-70.

50. Takahashi A, Kubo M, Ma H, Nakagawa A, Yoshida Y, Isono M, et al. Nonhomologous end-joining repair plays a more important role than homologous recombination repair in defining radiosensitivity after exposure to high-LET radiation. Radiat Res. 2014; 182:338-44.